γ decay from the quasicontinuum of ^{197,198}Au

F. Giacoppo,[1,*] F. L. Bello Garrote,[1] L. A. Bernstein,[2] D. L. Bleuel,[2] R. B. Firestone,[3] A. Görgen,[1] M. Guttormsen,[1] T. W. Hagen,[1] M. Klintefjord,[1] P. E. Koehler,[1,4] A. C. Larsen,[1] H. T. Nyhus,[1] T. Renstrøm,[1] E. Sahin,[1] S. Siem,[1] and T. Tornyi[1,5]

[1]*Department of Physics, University of Oslo, N-0316 Oslo, Norway*

[2]*Lawrence Livermore National Laboratory, 7000 East Avenue, Livermore, California 94550-9234, USA*

[3]*Lawrence Berkeley National Laboratory, 1 Cyclotron Road, Berkeley, California 94720-88R0192, USA*

[4]*Air Force Technical Applications Center, Patrick Air Force Base, Florida 32925, USA*

[5]*Institute of Nuclear Research of the Hungarian Academy of Sciences (MTA Atomki), H-4001 Debrecen, Hungary*

(Received 5 January 2015; revised manuscript received 30 March 2015; published 26 May 2015)

The average electromagnetic dipole response of levels in the quasicontinuum of ^{197,198}Au has been measured using (^{3}He,^{3}He$'$) and (d,p) reactions. The extracted γ-ray strength functions have been normalized according to three model assumptions for the nuclear spin distribution. An enhancement in the energy region $E_\gamma =$ 3.0–6.5 MeV is observed for both isotopes. The $E1$ component of such excess of strength is studied in detail for ^{198}Au and is interpreted as the pygmy dipole resonance with an energy centroid of 5.9(1) MeV and exhausts about 1% of the total integrated strength. The pygmy dipole resonance is shown to have a significant impact on the calculated ^{197}Au$(n,\gamma)^{198}$Au cross section.

DOI: 10.1103/PhysRevC.91.054327 PACS number(s): 25.40.Hs, 25.55.Ci, 25.20.Lj, 24.30.Gd

I. INTRODUCTION

The fast development of new technologies addressed to the design of nuclear reactors for energy production and nuclear waste transmutation requires accurate neutron cross section and activation measurements in order to update existing nuclear data libraries [1–4].

So far, most neutron cross sections, especially at thermal energies, have not been measured absolutely but relative to the standard ^{197}Au(n,γ) reaction. Gold is suitable for its monoisotopic stable form and its large thermal neutron capture. During the past four decades, a multitude of measurements based on different detection techniques have been carried out. A large experimental database is used for the evaluation of the cross section standards, published into the national nuclear data projects (USA, Europe, Japan, Russia, and China); the latest release is the European JEFF-3.2 [5–9].

The neutron capture cross section of ^{197}Au is also used as a standard for the laboratory measurement of the (n,γ) cross sections relevant in the study of the stellar s-process (slow neutron captures) which is responsible for about one half of the isotopic abundances in the mass region between Fe and Bi [10]. However, in spite of the increasing amount of high-quality experimental data, cross section calculations at stellar conditions are essential when the reaction path involves nuclides away from the valley of stability and branch-point nuclei.

Neutron capture rates are usually calculated within the statistical Hauser-Feshbach approach [11], with the assumption that the reaction occurs mainly through the formation of a compound nucleus. The quality of the calculations is sensitive to the input model parameters: (i) the optical model potential, (ii) the nuclear level density, and (iii) the γ transition probability. Often, the latter is the most crucial input and is usually determined, for high γ energies, from the inverse (γ,n) reaction applying the principle of detailed balance [12].

The nuclear level density and the γ transition probability, which for excited states in the quasicontinuum is usually expressed by the γ-ray strength function (γSF), are very sensitive to the spin distribution of the residual nucleus. This is commonly expressed by a Gaussian-like formula with a dispersion parameter σ, the so-called spin cutoff, that depends on the effective moment of inertia of the nucleus [13]. For transitional nuclei in the proximity of shell closure, such as the Au isotopes, previous studies based on the analysis of the isomeric cross section ratio, indicate values close to the rigid-body moment of inertia for σ [14].

In this work we present new measurements of the γSF of ^{197,198}Au. In particular, we test different spin distributions for the absolute normalization of the γSF. These data, together with the experimental level densities determined simultaneously in the same experiment [15] by applying the Oslo method [16,17], are used as input in the statistical calculations of the ^{197}Au$(n,\gamma)^{198}$Au cross section. Only when both inputs are experimentally determined and consistently normalized can the resulting calculations reproduce the ^{197}Au capture cross section data available in literature.

Another reason that motivates this experimental study concerns the understanding of nuclear reaction mechanisms occurring in a stellar plasma. Such environmental conditions are reproduced at the National Ignition Facility (NIF) [18], where a frozen deuterium-tritium (DT) target enclosed in a gold hohlraum is bombarded with intense laser beams. This scenario portrays the extreme temperature and density conditions of exploding stars. Recent measurements of the neutron activation of gold in the NIF hohlraum suggest that highly excited quasicontinuum states in ^{196}Au and ^{198}Au are formed via the ^{197}Au$(n,2n)$ and the ^{197}Au(n,γ) reactions, respectively, in thermal equilibrium with the environment [19,20]. They might interact with the surrounding high energy density plasma before γ decay and, as a consequence, the relative

*francesca.giacoppo@fys.uio.no

population of the $J^\pi = 12^-$ isomer and the $J^\pi = 2^-$ ground state in gold might be altered. This prestatistical decay nuclear plasma interaction (NPI) could modify neutron-capture rates in astrophysical plasmas, therefore affecting the production of heavy elements in certain astrophysical settings. The NPI rates are in turn highly sensitive to nuclear level densities and γSFs. The recently published level density of ^{198}Au [15], together with the γSF results presented in this work may give additional information on the NPI mechanism on excited nuclear states.

This article is organized as follows. In Sec. II the experimental procedure and the analysis method are presented. Details about the absolute normalization of the γSF are discussed in Secs. III and IV. The latter includes also comparisons with other experimental results and model predictions. Section V is dedicated to the (n,γ) cross section calculations. A summary and the conclusions are finally drawn in Sec. VI.

II. EXPERIMENTAL SETUP AND DATA ANALYSIS

Excited states of ^{197,198}Au were populated through the $(^3\mathrm{He},^3\mathrm{He}')$ scattering reaction and the (d,p) transfer reaction, respectively, at the Oslo Cyclotron Laboratory (OCL). The ^{3}He and deuteron beams had incident energies of 34.0 and 12.5 MeV, respectively. The two ^{197}Au targets irradiated during the experiments had a thickness of about 1.9 mg/cm^2 and were mounted on a ^{nat}Ta frame. The light ejectiles were detected in the SiRi (Silicon Ring) particle detector [21] in coincidence with the γ rays emitted by the residual nucleus, that were measured with the CACTUS spectrometer [22]. The SiRi detector consists of eight trapezoidal Si crystals 1550 μm thick mounted in an annular configuration, each one coupled to a eightfold segmented thin Si detector (130 μm thick). Thus, a total of 64 independent ΔE-E telescopes are available for particle identification and energy measurements. The SiRi telescopes were placed at 5 cm distance from the target and covered the scattering angle window $\theta \in [126^\circ,140^\circ]$ with a resolution of $\Delta\theta = 2^\circ$. For these experiments, the γ-ray spectrometer was composed by 26 $5'' \times 5''$ NaI(Tl) γ-ray detectors mounted on a spherical frame. A conical lead collimator with a thickness of 10 cm is placed at the front face of each NaI(Tl). For 26 NaI(Tl) detectors in operation, CACTUS covers a total solid-angle of 16.2% out of 4π and has a total detection efficiency of 14.1(1)% at $E_\gamma = 1332$ keV.

Particle-γ coincidences were recorded event by event in a time window of about 1.2 μs. In order to sort out the true coincidence events, a gate is set at the prompt peak of the measured time spectra which has a resolution of $\sim$12 ns. The residual nucleus excitation energy E is reconstructed from the measured energy and angle of the light ejectile, taking into account the reaction kinematics and Q value. A resolution of $\Delta E = 150$ and 200 keV was obtained for the reaction with d and ^{3}He beams, respectively. A two-dimensional distribution of the emitted γ rays versus excitation energy is then derived. The *unfolding method* is used to correct the γ spectra for the known CACTUS response functions [23]. With this method, the resulting γ spectra have statistical fluctuations similar to that of the raw γ distributions.

The γ-ray distribution includes all the generations of transitions emitted in the cascades from highly excited levels.

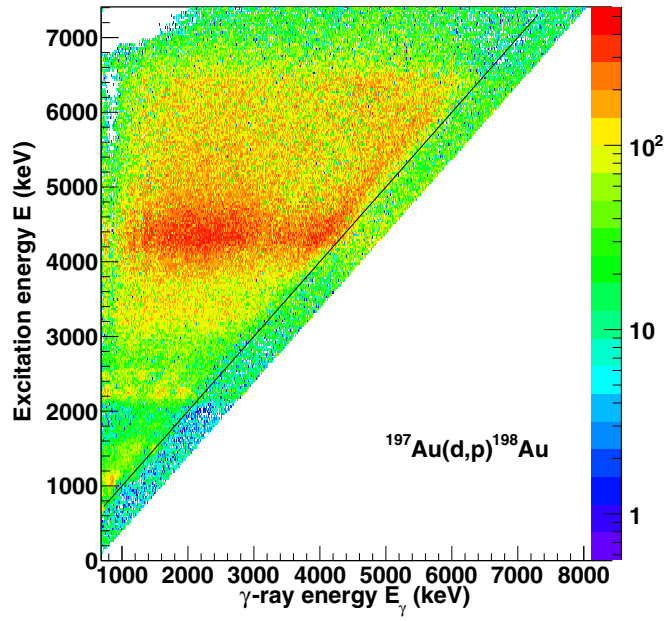

FIG. 1. (Color online) Excitation energy versus primary γ ray energy of ^{198}Au. The black diagonal line $E = E_\gamma$ defines the γ rays of highest energy within each excitation energy bin. The intensity of γ transitions drops in correspondence with the neutron separation energy $S_n = 6.512$ MeV.

In order to disentangle the primary γ rays from the cascades at a given initial energy E, the *first-generation method* is applied [24]. The distribution of primary γ rays for the excitation energy bin i is obtained by subtracting a weighted sum of all the γ distributions from the energy bins up to $i-1$, taking into account the average γ-ray multiplicity. The procedure is iterated $\sim$10 times in order to converge. The final weighting coefficients give directly the ith first generation spectrum. The first-generation method is based on the assumption that the γ-ray distribution is unchanged whether the initial excitation region is populated directly by the reaction or at an intermediate stage of the γ cascade. Generally, in the matrix of primary γ rays $P(E,E_\gamma)$ many levels are included within each energy bin (except at low excitation energies) which on average is populated with the same probability by the two possible ways. Once the matrix of primary γ rays $P(E,E_\gamma)$ tagged by excitation energy is built for ^{197,198}Au, it is possible to extract information on their level density and γSF.

Figure 1 shows the first-generation matrix of ^{198}Au with a pronounced diagonal line which corresponds to the direct decay to the low-lying excited states $(0^- - 4^-)$ in the range $\sim$250–400 keV. The ground state does not show an intense direct feeding from high-energy states. A high density of primary γ rays is clustered in the excitation energy window between 3.7 and 5.0 MeV where the (d,p) cross section is high.

When the γ emission is governed by statistical rules, it is possible to decompose $P(E,E_\gamma)$ into two independent functions of E_f (with $E_f = E - E_\gamma$) and E_γ [16]:

$$P(E,E_\gamma) \propto \rho(E - E_\gamma)\mathcal{T}(E_\gamma), \quad (1)$$

where $\rho(E_f)$ is the level density at the final excitation energy and $\mathcal{T}(E_\gamma)$ is the γ transmission coefficient. In the statistical regime, a compound state is formed during the reaction and the γ-decay probability is independent of the formation channel [25]. However, this is not the case at low excitation energy where the γ transitions strongly depend on the initial and final states and direct reactions can play an important role. We therefore restrict our analysis to the γ decay from initial excitation energies above 3 and 2 MeV for ^{197,198}Au, respectively.

Furthermore, the electromagnetic decay from the quasicontinuum is dominated by dipole transitions, which are independent of the excitation energy according to the generalized Brink-Axel hypothesis [26,27]. The latter states that collective modes built on the ground state or any excited states have equivalent properties regardless of the temperature of the state. It has been demonstrated that this assumption is not valid for reactions that involve high temperature and high momentum transfer [28]. Since, for the reactions studied in this work, the temperature of the residual nucleus is low and the spin populated represents a low and narrow distribution, the Brink-Axel hypothesis is assumed to be valid. In the next section we show that the direct decay from the quasicontinuum to the low-lying excited states observed in Fig. 1 does not undermine the assumptions of statistical decay and independence of excitation energy.

The functional form of both the level density and the γ transmission coefficient can be determined by a simultaneous least-χ^2 minimization of $P(E,E_\gamma)$ into the product $\rho(E-E_\gamma)\mathcal{T}(E_\gamma)$. For this product, infinitely many possible solutions generated by the transformations

$$\tilde{\rho}(E-E_\gamma) = A\mathrm{e}^{\alpha(E-E_\gamma)}\rho(E-E_\gamma), \tag{2}$$

$$\tilde{\mathcal{T}}(E_\gamma) = B\mathrm{e}^{\alpha E_\gamma}\mathcal{T}(E_\gamma), \tag{3}$$

can be obtained. The absolute level density and γ transmission coefficient are finally obtained for a given set of parameters A, B, and α determined by comparison with independent experimental data.

In particular the amplitude A and the slope α are deduced from the normalization of ρ to the density of known levels at low excitation energy [29] and to the value at the neutron separation energy $\rho(S_n)$. The latter is derived from the systematics of Ref. [30] for ^{197}Au and from the experimental average s-wave neutron resonance spacing D_0 taken from Ref. [31] for ^{198}Au. The spin is assumed to follow the expression [13]

$$g(J,\sigma) \simeq \frac{2J+1}{2\sigma^2} e^{-\frac{J(J+1)}{2\sigma^2}}. \tag{4}$$

Further details and final results on the level density of ^{197,198}Au have been presented in a separate work [15]. In this paper we focus on the γSF and the characterization of its resonance structures.

III. GAMMA STRENGTH FUNCTION

The γ-ray transmission coefficient $\mathcal{T}(E_\gamma)$ which has been extracted from the experimental data applying Eq. (1), is associated to the γSF $f(E_\gamma)$ by the relation

$$\mathcal{T}(E_\gamma) = 2\pi \sum_{XL} E_\gamma^{2L+1} f_{XL}(E_\gamma)$$

$$\approx 2\pi E_\gamma^3 [f_{E1}(E_\gamma) + f_{M1}(E_\gamma)], \tag{5}$$

where X and L stand for the electromagnetic character and the multipolarity of the γ ray, respectively. Only dipole transitions ($L=1$) are taken into account as the dominant γ decay channel in the quasicontinuum. This approximation is justified by the fact that the contribution of $L=2$ γ radiation is of minor importance [32,33].

The slopes of the transmission coefficient $\mathcal{T}(E_\gamma)$ and $\rho(E_f)$ are related though the common parameter α. In order to obtain the normalized γSF, the parameter B in Eq. (3) has to be determined using the following expression:

$$\langle \Gamma_\gamma(S_n, J^\pi)\rangle = \frac{1}{4\pi\rho(S_n, J_i^\pi)} \int_0^{S_n} dE_\gamma B\mathcal{T}(E_\gamma)$$

$$\times \rho(S_n - E_\gamma) \sum_{J_f} g(S_n - E_\gamma, J_f), \tag{6}$$

where the average total radiative width $\langle\Gamma_{\gamma 0}\rangle$ at S_n is extracted from s-wave neutron resonances [31]. The initial spin and parity J_i^π is connected to the spin and parity of the target nucleus I_t^π in the (n,γ) reaction by the expression $J_i^\pi = I_i^\pi \pm 1/2$. The sum is extended to all the final states with spin $J_f = J_i, J_i \pm 1$. However, the spin distribution of the nucleus itself is expressed by Eq. (4) and both positive- and negative-parity levels are assumed to contribute with the same probability. Here we adopt the energy-dependent empirical expression for the spin cutoff σ (EB2009) proposed in Ref. [30]. It is interesting to mention that ρ is the experimental level density and the factor $1/\rho(S_n, J_i^\pi)$ corresponds to the neutron resonance spacing D_0. Therefore, $D_0 = 15.5(8)$ eV

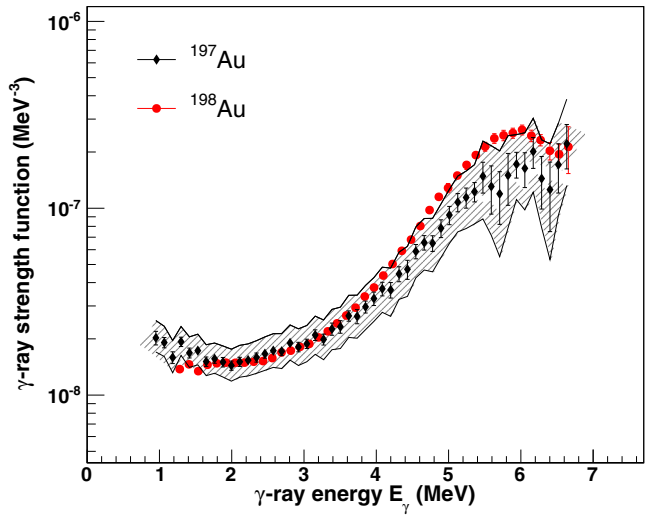

FIG. 2. (Color online) γSFs of ^{197}Au (black filled diamonds) and ^{198}Au (red filled circles). For the odd-mass isotope, in addition to the statistical error bars, a large systematic error (hatched area between black lines) is included, due to the uncertainties of the absolute normalization.

and $\langle\Gamma_{\gamma 0}\rangle = 128(6)$ meV [31] are entered in Eq. (6) to normalize the γSF of ^{198}Au. Unfortunately, no experimental values of D_0 and $\langle\Gamma_{\gamma 0}\rangle$ are available for ^{197}Au, since ^{196}Au is not a stable target for the (n,γ) reaction.

As described in Ref. [15], the level density of ^{197}Au at S_n is estimated by comparing the systematics of von Egidy and Bucurescu [30] for neighboring isotopes with $\rho(S_n)$ obtained from available D_0 experimental values. This procedure allowed us to assess $\rho(S_n) = 4.0(12) \times 10^6$ MeV^{-1} and then $D_0 = 3.03$ eV with a large uncertainty of $\approx$43%. The average γ width of ^{197}Au is taken close to the value of ^{198}Au, $\langle\Gamma_{\gamma 0}\rangle = 142$ meV. This is justified by the fact that the γSFs of both Au isotopes are expected to be scaled down consistently in order to get normalized distributions with similar amplitude. Photoneutron cross section data of collective excitations in atomic nuclei confirm that the dipole electromagnetic response of close-lying isotopes shows in general the same features and is only slowly dependent on the neutron number [34].

Figure 2 shows the normalized total γSFs of ^{197,198}Au. For the even-odd isotope a large error band takes into account the uncertainty due to the normalization, which is mainly affected by the uncertainties in the determination of the level density slope from the deduced estimate of D_0. This data set is also characterized by larger statistical errors compared to the other isotope, ^{198}Au, especially for $E_\gamma \geqslant 5.4$ MeV. Nevertheless, within the uncertainties, a broad enhancement in the γ energy region between 4.5 and 6.4 MeV is observed in the γSF of ^{197}Au. This resonant structure is measured with better accuracy for the odd-odd isotope ^{198}Au.

The striking enhancement has been first defined as an "anomalous bump" by Bartholomew *et al.* who observed a systematic high intensity of γ rays with a mean energy of $E_\gamma \sim 5$ MeV in the decay spectra from thermal neutron capture and (d,p) reactions on several heavy nuclei [35,36]. Later, this structure was identified as a concentration of $E1$ transitions with a total strength seemingly dependent on the excess of neutrons forming a skin around the isospin-saturated core of protons and neutrons. It is frequently denoted as the pygmy dipole resonance (PDR) [37].

As mentioned in Sec. I, results from neutron-induced reactions suggest that the quasicontinuum of ^{198}Au includes high-spin levels with an average distribution depending on the effective moment of inertia of the nucleus [14]. In addition, gold isotopes are characterized by high-spin isomer levels even at relatively low excitation energies [29]. The effective moment of inertia assumes the value of the rigid-body already when few free quasiparticles are available in the levels close to the Fermi surface and pairing correlations fade out. Therefore, an alternative normalization of the γSF of ^{198}Au is proposed considering an energy-dependent spin distribution that reaches the rigid-body value at S_n (RMI) [38]. Another option is given by the Hartree-Fock-Bogoliubov plus combinatorial (HFB+comb) method which provides a spin-dependent level density with an average spin distribution centered at $\sim 7\hbar$ at the neutron separation energy [39]. Figure 3 shows a comparison of the three adopted parametrizations for σ and the resulting spin distributions at $S_n = 6.512$ MeV.

However, the d-induced transfer reaction may not populate the levels with the highest spin, giving only a transfer momentum of $\Delta L = 4$–$5\,\hbar$, which could affect the experimental primary γ spectra $P(E,E_\gamma)$. Following the procedure described in Ref. [40], the distribution of primary γ rays is decomposed in the product of a reduced level density $\rho_{red}(E_f)$ and the transmission coefficient $\mathcal{T}(E_\gamma)$ which should not be affected by the populated spin. The level density

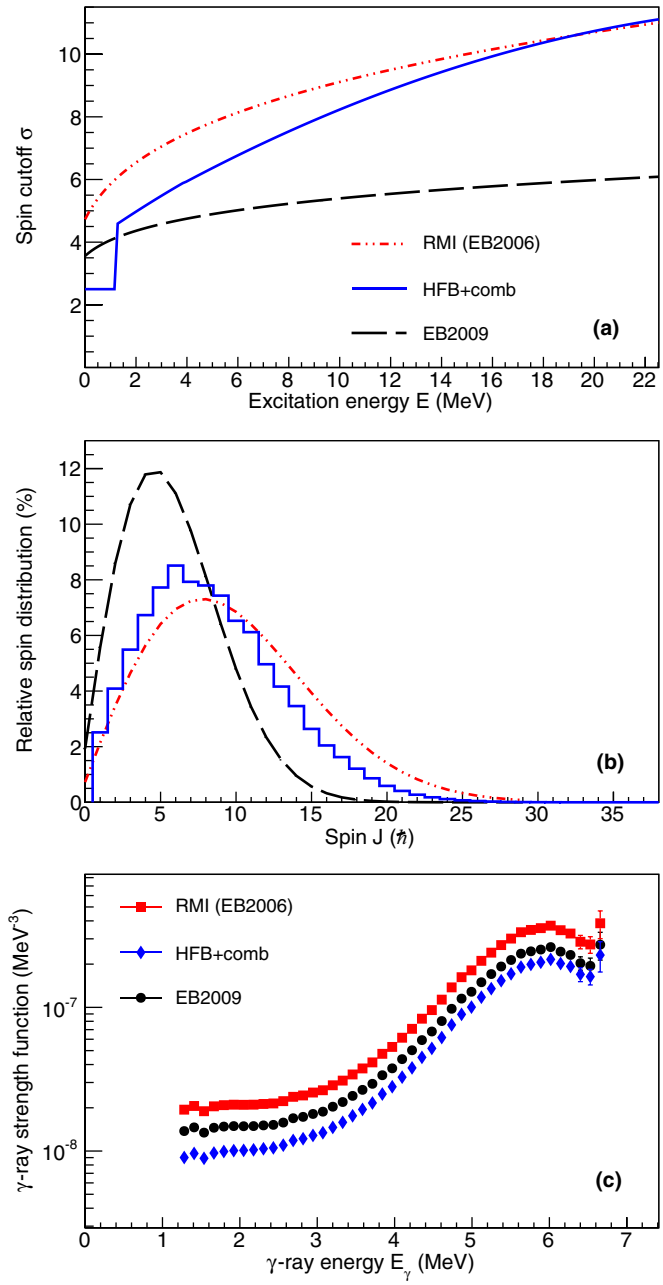

FIG. 3. (Color online) (a) Spin cutoff distributions as a function of the excitation energy chosen for the normalization of the γSF of ^{198}Au: the rigid moment of inertia (RMI, EB2006) formula as provided by von Egidy and Bucurescu [38], the latest energy-dependent formula from the same authors (EB2009) [30], and the spin cutoff from a microscopic model for the level density (HFB+comb) [39]. (b) The spin distributions at $S_n = 6.512$ MeV and (c) the normalized γSFs corresponding to the three models adopted for $g(J,\sigma)$.

TABLE I. Spin input parameters used to extract the level density and γSF of ^{198}Au.

Model	$\sigma(S_n)$	$\rho(S_n)$ (10^6 MeV^{-1})	$\rho_{red}(S_n)$ (10^6 MeV^{-1})
EB2009	5.08	0.91(17)	
RMI	8.43	2.37(47)	0.95
HFB+comb	6.97	1.65(32)	0.90

$\rho_{red}(E_f)$ is normalized to a lower value at S_n, corresponding to 40% and 50% of $\rho(S_n)$ calculated using the RMI and HFB+comb spin models, respectively (see Table I). The resulting γSFs are displayed in Fig. 3(c): the broader RMI spin curve generates a γSF which is about 40% higher than the "reference" case (EB2009) corresponding to the narrower curve for $g(J,\sigma)$. When the spin distribution from the microscopic calculations (HFB+comb) is taken into account in Eq. (6), a ~20% reduction of the absolute value of the γSF is obtained.

In the following we will consider the RMI and HFB+comb γSFs as the higher and lower limit, respectively, for the absolute γSF of ^{198}Au, due to the uncertainties on the nuclear spin in the quasicontinuum. In the next section the γSF of ^{198}Au will be compared with other experimental data from photoproduction measurements and with model predictions.

Now we turn our attention to the assumption made when applying the Oslo method, namely the condition of a decay process which is statistical in nature. If this hypothesis is correct, *selected* γSFs extracted from subsets of initial and/or final excitation energies should correspond to the total γSF within the limit of Porter-Thomas fluctuations [41], which can be more pronounced when the subset of γ transitions is small.

Figure 4 shows the γSFs for two 0.38-MeV-wide bins of final excitation energies centered at 0.3 and 1.1 MeV, extracted with the same procedure as in Ref. [42]. In the first case a certain contribution of direct decay from the quasicontinuum is included (as observed in Fig. 1) whereas in the second case a more uniform patter of γ transitions feed these final levels. The dotted line represents the total γSF extracted for the whole final excitation energy window. The solid lines correspond to the selected γSFs calculated for final energies below 0.51 MeV and in the region $E_f \in [0.51,1.15]$ MeV. The selected γSF in the former energy window deviates from the total distribution for $E_\gamma < 3.3$ MeV. The excess observed at $E_\gamma = 4.0$–4.5 MeV corresponds to the direct feeding from the quasicontinuum. In Fig. 4(b) the total and selected γSF are in good agreement within a difference of 10%. Ultimately, selected γSFs can display a certain variation, depending on the chosen initial and final excitation energy window, especially when transitions to the lowest excited levels are taken into account. However, the variation due to the direct feeding from the quasicontinuum is of only ~20%, suggesting that the Porter-Thomas fluctuations are relatively small due to the high number of γ transitions involved in the decay process. From Fig. 4 we conclude that the Brink-Axel hypothesis is surprisingly well accounted for even for decay to the lowest excitation energies.

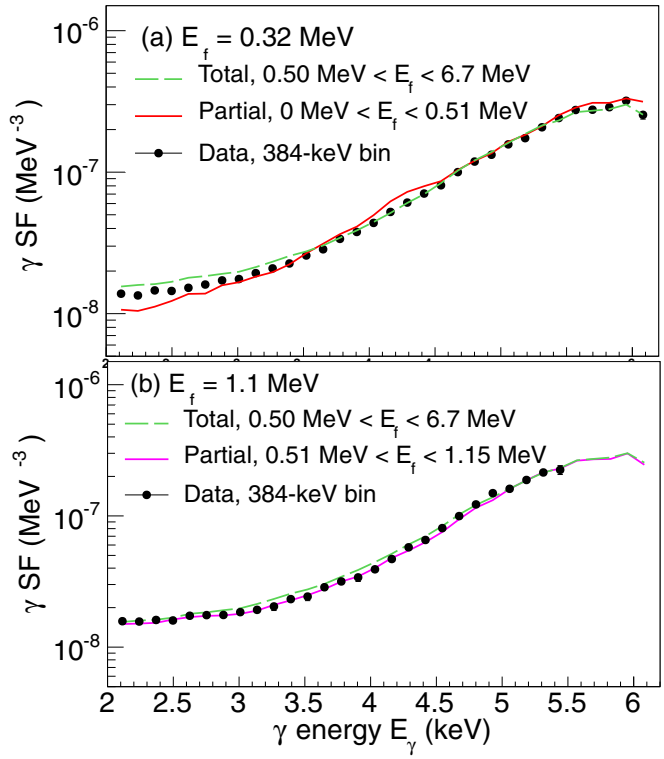

FIG. 4. (Color online) The γSF of ^{198}Au for two final excitation energies (black filled circles) $E_f = 0.32$ MeV (a) and $E_f = 1.1$ MeV (b). Comparison with the total γSF (green dashed line) and the selected γSFs (solid red and violet lines) extracted for a narrow window of final excitation energies centered at the chosen E_f.

IV. COMPARISON WITH OTHER DATA AND MODELS

Generally, the Oslo method provides total γSFs in the energy region below the neutron separation energy. It is very useful to combine this information with photoneutron cross-section data which characterize the energy window of the isovector giant dipole resonance (GDR). The (γ,n) cross section $\sigma(E_\gamma)$ can be converted into γSF through the relation

$$f(E_\gamma) = \frac{1}{3(\pi\hbar c)^2}\frac{\sigma(E_\gamma)}{E_\gamma} \quad (7)$$

assuming the γ transition to be of dipole nature.

In literature, there are available partial cross sections of (γ,n) and $(\gamma,2n)$ reactions on ^{197}Au measured by using monoenergetic γ rays from positron annihilation in flight (PAIF). These data have been collected at two research laboratories, the Lawrence Livermore National Laboratory (LLNL) [43,44] and Saclay [45]. Due to different methods applied to determine the neutron multiplicity, there are discrepancies among the results from the two institutes. In particular, for the ^{197}Au(γ,n) cross section a variation of ~8% is measured around the GDR peak region. A later photoactivation experiment, performed at the S-DALINAC (Darmstadt), has provided more precise data for energies close to the (γ,n) threshold [46]. Recent photoneutron cross section measurements have been carried out at the National Institute for Advanced Industrial Science and Technology (AIST) with monoenergetic photon beams

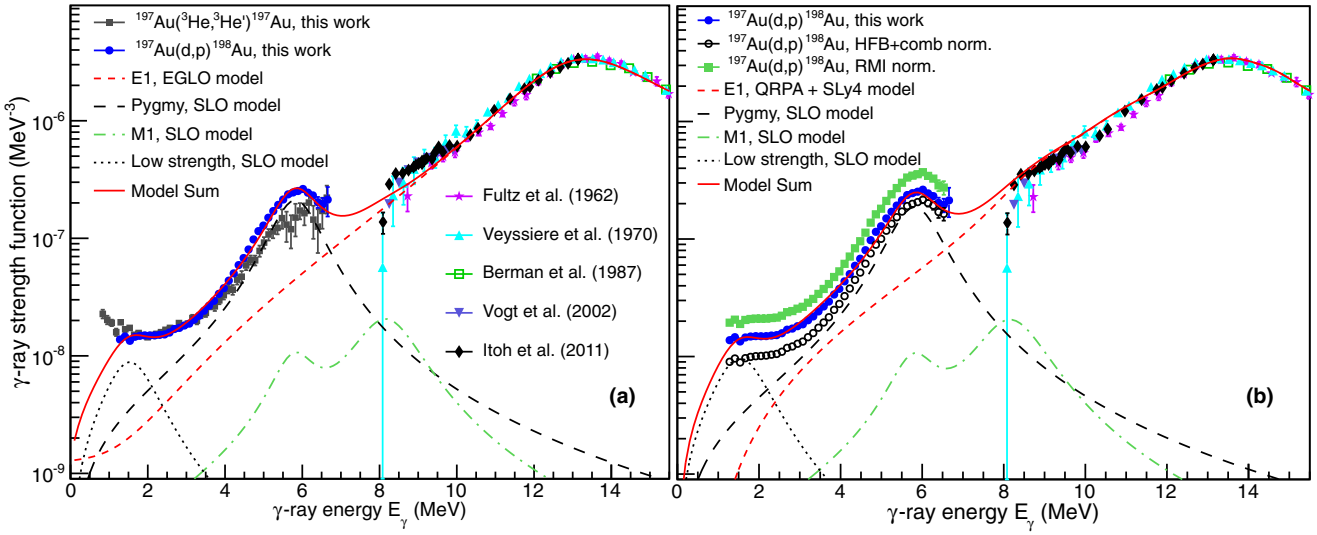

FIG. 5. (Color online) (a) Comparison between the γSF of ^{197,198}Au from this work and from (γ,n) reactions [43–47]. The data are modeled with a combination of the EGLO model and four SLO components (model A). (b) Three possible normalizations for the γSF of ^{198}Au are compared (see text). Another model parametrization is proposed, based on the QRPA approach (red dashed line) for the $E1$ strength (model B).

produced with a more advanced technique: laser Compton backscattering (LCS) [47]. Thanks to the use of a highly efficient neutron detector for direct neutron counting and to the improved energy resolution, the ^{197}Au(γ,n) cross section has been determined with considerably reduced uncertainty from the neutron threshold up to 14.5 MeV where the $(\gamma,2n)$ channel opens. All the measurements agree well below 10 MeV, but give different cross sections at the GDR peak.

The five data sets, expressed as γSFs, are included in Fig. 5 and compared with the data of this work. The aim of this comparison is to cross-check the accuracy of the normalization and to assess the contribution of the tail of the GDR to the total γ strength in the energy region below the neutron threshold.

In Fig. 5(a) the GDR is reproduced by the enhanced generalized Lorentzian (EGLO) model [32]. This model is customized to give a suitable description both of the photoabsorption cross section data and the γ strength below S_n. The free model parameters, listed in Table II, are the centroid energy E_{E1}, the width Γ_{E1}, and the cross section σ_{E1}. They are chosen among the values suggested in Refs. [43–47] and give a reliable description of the photoneutron data between $E_\gamma \sim 10.0$ MeV and the resonance peak. However, this parametrization underestimates the γSF at the neutron threshold. The model includes a nonzero limit for the low-energy region which depends on the nuclear temperature T_f at the final state [48] that is here assumed as a constant parameter to be consistent with the Brink-Axel hypothesis. This extrapolation gives a reasonable estimate of the GDR tail in the region below the neutron binding energy and is considered as a baseline for the total γSF.

Between 3.0 and 6.5 MeV the γSF shows a rapid increase of slope and a maximum at about 5.8 MeV, contributing with 31.4 MeV mb to the energy integrated strength (EWSR). It is not trivial to characterize the observed excess of strength since competing contributions due to spin-flip transitions and electric dipole decay overlap in this energy region. An effective attempt to quantify the spin-dependent γSF is based on a comparison with the experimental results available for many nuclei in the same mass region [49]. The magnetic dipole response of atomic nuclei consists of a weak isoscalar term and a stronger isovector component, which are related to separate neutron and proton spin-flip excitations and their residual interaction. From experimental studies of rare-earth, actinide, and closed-shell nuclei such as ^{208}Pb, a simple $cA^{-1/3}$ law has been deduced (with $c = 34$ and 44 MeV for the isoscalar and isovector components, respectively) for the energy centroids of the double-humped $M1$ strength ([49,50] and references therein). The total magnetic strength is estimated to be $B(M1) \geqslant 20\mu_N^2$ for ^{198}Pt from microscopic calculations [51]. Assuming the same amount of strength for ^{198}Au, we allocate 20% to the isoscalar component. In Fig. 5 the $M1$ strength is included as the sum of two standard Lorentzian (SLO) functions [31]; the cross-section and width parameters are chosen in accordance to the available existing data overviewed in Ref. [50]. With the present model description, the remaining observed strength is attributed to the $E1$ pygmy resonance (see Table II) and exhausts 1.1% of the total $E1$ strength.

Another excess of strength is observed at the very low tail of the γSF and is reproduced by a weak SLO distribution for ^{198}Au. For $E_\gamma = 1.3$–3.1 MeV the γSF of the odd-odd gold isotope has a roughly constant behavior. The strength of ^{197}Au is also added in Fig. 5(a) and suggests the inset of an enhancement for $E_\gamma < 1.5$ MeV. Mid-shell even-even deformed nuclei exhibit a pronounced collective excitation due to the orbital component of the magnetic strength, the so-called scissors mode [50]. Such resonance is observed also in deformed odd-mass nuclei with a strength expected from the adjacent even-even isotopes but with a significant fragmentation [52]. The systematics of the $M1$ scissors mode in the quasicontinuum of actinide isotopes confirm the common

TABLE II. Resonance parameters used for the model description of the γSF of ^{198}Au according to the EGLO+SLOs (model A) and QRPA+SLOs (model B) options described in the text and shown in Fig. 5.

	GDR				PDR			$M1$ spin-flip						Low-energy tail		
	E_{GDR} (MeV)	Γ_{GDR} (MeV)	σ_{GDR} (mb)	T_f (MeV)	E_{E1} (MeV)	Γ_{E1} (MeV)	σ_{E1} (mb)	$E_{M1,1}$ (MeV)	$\Gamma_{M1,1}$ (MeV)	$\sigma_{M1,1}$ (mb)	$E_{M1,2}$ (MeV)	$\Gamma_{M1,2}$ (MeV)	$\sigma_{M1,2}$ (mb)	E (MeV)	Γ (MeV)	σ (mb)
A	13.86	4.81	505	0.15	5.86	$1.38^{+0.07}_{-0.18}$	$14.20^{+6.30}_{-2.00}$	5.83	1.20	0.55	8.21	1.80	1.90	1.70	1.50	$0.16^{+0.08}_{-0.08}$
B					5.86	$1.38^{+0.07}_{-0.28}$	$12.60^{+6.60}_{-2.10}$	5.83	1.20	0.55	8.21	1.80	1.90	1.70	1.50	$0.18^{+0.08}_{-0.07}$

general pattern (summed strength and average centroid energy) for odd-mass, even-even, and odd-odd nuclei [40,53,54]. This resonance has also been observed in γ-soft nuclei such as ^{194,196}Pt [55,56], where the $M1$ strength is not concentrated in few strong states, but is fragmented over several levels due to the interplay of complex mixed-symmetry quasiparticle configurations [50]. According to the results for the Pt isotopes, a weak and fragmented scissors mode could be present also in the γSF of ^{197,198}Au at $E_\gamma \approx 2.5$–3.5 MeV.

In addition, in previous experiments performed at OCL it has been measured a low-energy plateau or even an "upbend" in the γSF of nuclei close to stability with $A < 140$ [57]. The current theoretical descriptions of this enhanced probability for low-energy γ decay in the quasicontinuum disagree on its electromagnetic character [58–60], whereas its multipolarity has been established experimentally to be of dipole nature in ^{56}Fe [33]. Among the different theoretical interpretations, it is foreseen that this phenomenon is mainly due to $M1$ $0\hbar\omega$ transitions and should be common to all the medium-mass and heavy nuclei throughout the nuclear chart [60], but could be "hidden" in the tail of higher-energy collective modes.

In Fig. 5(b) a microscopic approach based on the quasiparticle random-phase approximation (QRPA) with the SLy4 Skyrme force is chosen to describe the isovector $E1$ strength [61]. Following the recommendations given by the authors, a shift $E_{\rm shift} = 0.5$ MeV and a scaling $f^{\rm norm} = 0.95$ are applied in order to adjust the calculations to the GDR peak position and strength. This model overestimates the GDR tail above the neutron threshold and gives a higher baseline for the resonances observed below S_n. The model parameters used to fit the experimental data are also listed in Table II as model B. In this case, the excess of strength between 3.0 and 6.5 MeV assumes the low-limit of 28.0 MeV mb.

In the same figure are also shown the lowest and highest limit of the γSF of this work. Considering the two model fits, the excess of strength in the PDR region could be estimated to be $29.7^{+17.2}_{-10.6}$ MeV mb corresponding to $\sim 1.0^{+0.6}_{-0.4}$ % of the total integrated strength.

V. CALCULATIONS OF THE (n,γ) CROSS SECTION

The detailed study of the γSF of ^{198}Au in the quasicontinuum can be exploited to perform accurate statistical calculations of the ^{197}Au$(n,\gamma)^{198}$Au cross section with the reaction code TALYS [62]. The impact of near-threshold structures, as the observed pygmy resonance, will be discussed. These findings have direct consequences in the understanding of the s-process nucleosynthesis. Since the Hg isotopes are formed in the β decay of ^{198}Au, it is important to assess the relative strength of the ^{197}Au(n,γ) reaction and the ^{198}Au $\rightarrow$ ^{198}Hg $+ e^- + \bar{\nu}_e$ decay in stellar environments.

For the TALYS inputs we have used information of the experimental level density [15] and the γSF presented in this work. The three normalization options discussed previously in the text, related to the model assumptions for the nuclear spin distribution, are taken into account. The level density of ^{198}Au is well reproduced by the phenomenological constant temperature formula with parameters $T = 0.67$ and 0.61 MeV and $E_0 = -2.42$ and -2.10 MeV using the EB2009 and RMI normalizations, respectively. A tabular format, consistent with the default models implemented in TALYS libraries, is provided. For the HFB+comb normalization, the input table is obtained by decomposing the experimental total level density with regard to the spin distribution provided by the model. As discussed in Ref. [15], there is poor agreement between the concave curvature of the model total level density and the logarithmic functional form of the experimental distribution. The γSFs presented in Fig. 5(b) are expressed as a combination of EGLO and SLO functions, with the low-energy tail assumed to be of magnetic character. For the neutron optical model we have tested both the default option of TALYS, i.e., the local and global parametrizations of Koning and Delaroche (OMP) [63], and the semimicroscopic optical model of Jeukenne, Lejeune, and Mahaux (JLM) [64]. A maximum difference of 10% is obtained when one or the other model are chosen. Finally, we preferred the dispersive OMP potential with local parameters which gives the lowest (n,γ) cross section at incident neutron energies $E_n < 100$ keV and is in better agreement with the available experimental data, as will be shown below. The calculations reproduce well the neutron resonance spacing D_0 and the average γ width $\langle\Gamma_{\gamma 0}\rangle$, within the uncertainties of the experimental reference values [31]. It is significant to stress that such a good agreement has been obtained without applying any further normalization to the experimental input γSFs (the option $\rm G_{norm} = 1$ is set in TALYS).

In the following, the accuracy of the calculations is discussed through a comparison with experimental cross sections. In particular, recent measurements performed at the n_TOF facility at CERN explore the unresolved resonance region from $E_n = 5$ to 400 keV [65]. Older data which map the (n,γ) cross section in the neutron energy window from 100 keV to 5 MeV are also included [66–72]. In Fig. 6 the calculations are given by colored lines. A general good agreement is obtained for all the input sets; the major discrepancy concerns the cross section close to 1 MeV. The low-energy ($E_\gamma < 100$ keV) distribution is dominated by s-wave neutrons which populate rather low-spin

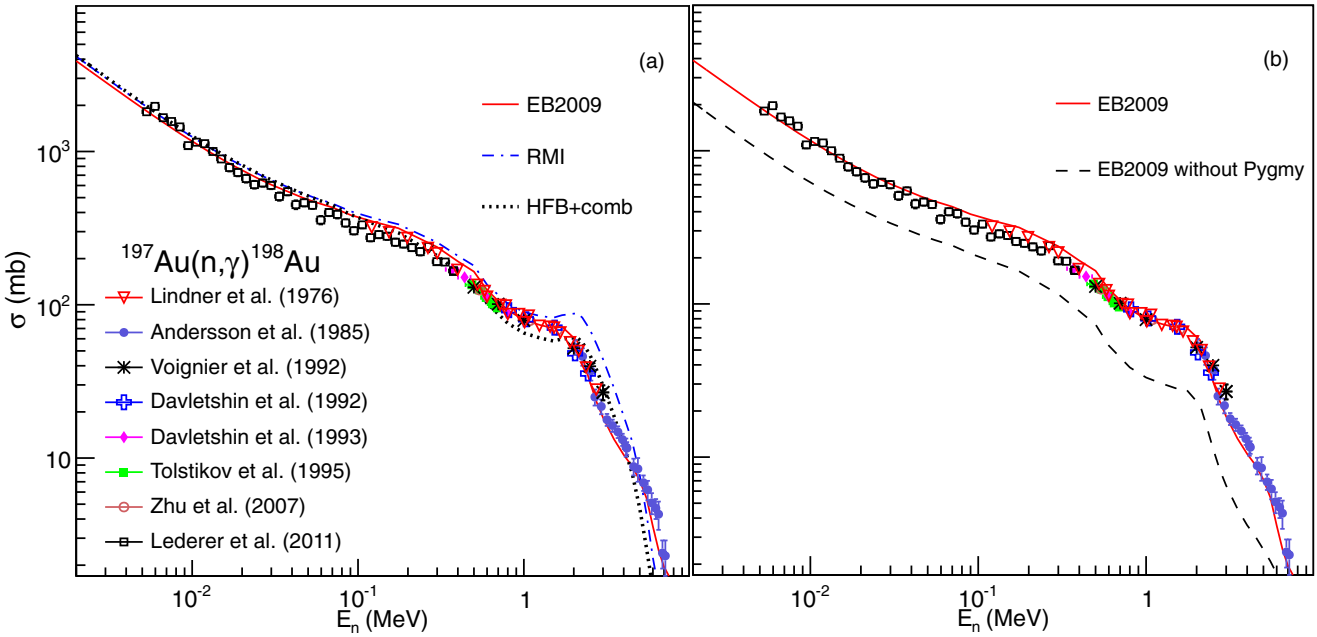

FIG. 6. (Color online) (a) Calculated ^{197}Au$(n,\gamma)^{198}$Au cross section using three sets of level densities and γSFs obtained from the normalization of the experimental data presented in this work assuming different spin distributions for ^{198}Au. (b) Calculated neutron capture cross section for ^{197}Au using the EB2009 inputs, with (red line) and without (dashed black line) including the PDR contribution in the γSF. The predictions are compared with measured data from Refs. [65–72].

states of the compound nucleus ^{198}Au. At higher energies p-wave neutrons can access levels with higher spins. However, the spin structure of ^{198}Au in the quasicontinuum seems to be dominated by low-spin states, since the inputs with the adopted low-spin distribution (EB2009) reproduce better the experimental cross section. As shown in Fig. 3(b), the EB2009 normalization corresponds to a spin distribution at S_n peaked at 4–5 $\hbar$; instead the RMI and HFB+comb spin curves have suppressed relative intensities for the low-spin values. The calculations compared in Fig. 6 suggest that, although a wide tail of high-spin values is foreseen for the levels in the quasicontinuum of ^{198}Au, their relative intensity should be low with respect to more dominant low-spin values.

In order to investigate the impact of the pygmy dipole resonance on the evaluation of the neutron capture cross section for ^{197}Au, the EB2009 calculations are displayed again in Fig. 6(b). When the PDR strength is not included in the input γSF, a dramatic underestimation of the (n,γ) cross section is obtained (∼46% below $E_n = 100$ keV and up to ∼65% at 4 MeV). Since the observed resonance is quite broad and located in the proximity of the particle threshold, a high portion of the primary γ transitions will correspond to γ rays with $E_\gamma = 4$–6 MeV. Such a consideration is of fundamental importance when neutron capture cross sections and reaction rates are calculated for r- and s-process nuclei far from stability for which experimental data are not available. Therefore, model calculations of the γSF should be carefully validated for nuclei close to stability through direct comparison with experimental data. At the same time, well-founded models of the excitation modes in atomic nuclei are highly desirable to allow for a proper prediction of the evolution of such collective behavior towards the drip lines.

VI. CONCLUSIONS

The γSF of ^{197,198}Au have been determined by means of particle-γ coincidence measurements. Three model assumptions for the nuclear spin distribution have been tested in order to extract the absolute γSF in the quasicontinuum of ^{198}Au. Although neutron-induced cross section data suggest that the effective moment of inertia of ^{198}Au corresponds to a rigid-body value already at the neutron separation energy, the present analysis suggests that levels in the quasicontinuum are dominated by lower spins ($J \leqslant 5\hbar$).

A broad excess of strength between $E_\gamma = 3.0$–6.5 MeV characterizes the γSF of both gold isotopes. This result confirms the long-known observation of a 5-MeV structure in the γ response of atomic nuclei by Bartholomew *et al.*. A detailed analysis using the Oslo method shows that this structure can be interpreted as a resonance with significant strength. According to the current knowledge of nuclear collective modes, it is partially due to spin-flip excitations and accounts mainly for the electric pygmy dipole resonance (PDR).

A small excess of strength is also observed below $E_\gamma = 3.0$ MeV, which cannot be accounted for by the model parametrization used to describe the low-energy tail of the GDR. As obseved in stable Pt isotopes, this structure suggests the presence of a weak (soft) $M1$ scissors mode. A possible contribution due to the upbend cannot be ruled out.

By including such a detailed description of the observed γSF of ^{198}Au in cross section calculations performed with the TALYS code, we have quantified the impact of the PDR as an increase of a factor of 2 in the ^{197}Au$(n,\gamma)^{198}$Au cross section for neutron energies in the keV – 5 MeV range. The

present study demonstrates the importance of a precise model description of low-energy resonances in the cross section calculations for nuclei far from stability where experimental data are not available.

ACKNOWLEDGMENTS

The authors thank J. C. Müller, E. A. Olsen, A. Semchenkov, and J. Wikne at the Oslo Cyclotron Laboratory for excellent experimental conditions.

[1] NEA-OEDC, Nuclear Energy Data 2013, available online at http://www.oecd-nea.org/ndd/pubs/2013/7162-bb-2013.pdf
[2] V. Artisyuk *et al.*, Prog. Nucl. Energy **50**, 314 (2008).
[3] G. Aliberti *et al.*, Ann. Nucl. Energy **33**, 700 (2006).
[4] G. Palmiotti and M. Salvatores, Ann. Nucl. Energy **52**, 10 (2013).
[5] M. B. Chadwick *et al.*, Nucl. Data Sheets **112**, 2887 (2011).
[6] JEFF 3.2 Joint Evaluated Fission and Fusion File, Nuclear Energy Agency, Paris, France (2014). Available online at: https://www.oecd-nea.org/dbforms/data/eva/evatapes/jeff_32/
[7] K. Shibata *et al.*, J. Nucl. Sci. Technol. **48**, 1 (2011).
[8] ROSFOND-2010 Library, Institute of Physics and Power Engineering, Obninsk, Russia (2010). Available online at http://www.ippe.ru/podr/abbn/libr/rosfond.php
[9] Z. G. Ge, Z. X. Zhao, and H. H. Xia, J. Korean Phys. Soc. **59**, 1052 (2011).
[10] F. Käppeler, Prog. Part. Nucl. Phys. **43**, 419 (1999).
[11] W. Hauser and H. Feshbach, Phys. Rev. **87**, 366 (1952).
[12] M. N. Harakeh and A. van der Woude, *Giant Resonances* (Oxford University Press, New York, 2001).
[13] T. Ericson, Adv. Phys. **9**, 425 (1960).
[14] M. Avrigeanu, V. Avrigeanu, M. Diakaki, and R. Vlastou, Phys. Rev. C **85**, 044618 (2012).
[15] F. Giacoppo *et al.*, Phys. Rev. C **90**, 054330 (2014).
[16] A. Schiller *et al.*, Nucl. Instrum. Methods Phys. Res., Sect. A **447**, 498 (2000).
[17] A. C. Larsen *et al.*, Phys. Rev. C **83**, 034315 (2011).
[18] G. H. Miller *et al.*, Nucl. Fusion **44**, S228 (2004).
[19] D. A. Shaughnessy *et al.*, Rev. Sci. Instrum. **85**, 063508 (2014).
[20] L. A. Bernstein *et al.*, Plasma Fusion Res. **9**, 4404101 (2014).
[21] M. Guttormsen *et al.*, Nucl. Instrum. Methods Phys. Res., Sect. A **648**, 168 (2011).
[22] M. Guttormsen *et al.*, Phys. Scr. T **32**, 54 (1990).
[23] M. Guttormsen *et al.*, Nucl. Instrum. Methods Phys. Res., Sect. A **374**, 371 (1996).
[24] M. Guttormsen *et al.*, Nucl. Instrum. Methods Phys. Res., Sect. A **255**, 518 (1987).
[25] A. Bohr and B. Mottelson, *Nuclear Structure*, Vol. I (Benjamin, New York, 1969).
[26] D. M. Brink, Ph.D. thesis, Oxford University, 1955.
[27] P. Axel, Phys. Rev. **126**, 671 (1962).
[28] A. Schiller and M. Thoennessen, At. Data Nucl. Data Tables **93**, 549 (2007).
[29] National Nuclear Data Center On-Line Data Service for the ENSDF database, http://www.nndc.bnl.gov/ensdf/
[30] T. von Egidy and D. Bucurescu, Phys. Rev. C **80**, 054310 (2009).
[31] T. Belgya *et al.*, *Handbook for Calculations of Nuclear Reaction Data*, RIPL-2, IAEA-TECDOC-1506 (IAEA, Vienna, 2006), available online at http://www-nds.iaea.org/RIPL-2/; R. Capote *et al.*, Reference Input Parameter Library RIPL-3 [Nucl. Data Sheets **110**, 3107 (2009)], available online at http://www-nds.iaea.org/RIPL-3/
[32] J. Kopecky and M. Uhl, Phys. Rev. C **41**, 1941 (1990).
[33] A. C. Larsen *et al.*, Phys. Rev. Lett. **111**, 242504 (2013).
[34] S. S. Dietrich and B. L. Berman, At. Data Nucl. Data Tables **38**, 199 (1988).
[35] B. B. Kinsey and G. A. Bartholomew, Phys. Rev. **93**, 1260 (1954).
[36] G. A. Bartholomew, E. D. Earle, J. Ferguson, and I. Bergqvist, Phys. Lett. B **24**, 47 (1967).
[37] D. Savran *et al.*, Prog. Part. Nucl. Phys. **70**, 210 (2013).
[38] T. von Egidy and D. Bucurescu, Phys. Rev. C **72**, 044311 (2005); **73**, 049901(E) (2006).
[39] S. Goriely, S. Hilaire, and A. J. Koning, Phys. Rev. C **78**, 064307 (2008).
[40] M. Guttormsen *et al.*, Phys. Rev. C **89**, 014302 (2014).
[41] C. E. Porter and R. G. Thomas, Phys. Rev. **104**, 483 (1956).
[42] M. Guttormsen *et al.*, Phys. Rev. C **83**, 014312 (2011).
[43] S. C. Fultz *et al.*, Phys. Rev. **127**, 1273 (1962).
[44] B. L. Berman, R. E. Pywell, S. S. Dietrich, M. N. Thompson, K. G. McNeill, and J. W. Jury, Phys. Rev. C **36**, 1286 (1987).
[45] A. Veyssiere *et al.*, Nucl. Phys. A **159**, 561 (1970).
[46] K. Vogt *et al.*, Nucl. Phys. A **707**, 241 (2002).
[47] O. Itoh *et al.*, J. Nucl. Sci. Technol. **48**, 1 (2011).
[48] S. G. Kadmenskii *et al.*, Yad. Fiz. **37**, 277 (1983) [Sov. J. Nucl. Phys. **37**, 165 (1983)].
[49] A. Richter, Prog. Part. Nucl. Phys. **34**, 261 (1995).
[50] K. Heyde, P. von Neumann-Cosel, and A. Richter, Rev. Mod. Phys. **82**, 2365 (2010).
[51] C. De Coster, K. Heyde, and A. Richter, Nucl. Phys. A **542**, 375 (1992).
[52] J. Enders, N. Huxel, P. von Neumann-Cosel, and A. Richter, Phys. Rev. Lett. **79**, 2010 (1997).
[53] M. Guttormsen *et al.*, Phys. Rev. Lett. **109**, 162503 (2012).
[54] T. G. Tornyi *et al.*, Phys. Rev. C **89**, 044323 (2014).
[55] P. von Brentano *et al.*, Phys. Rev. Lett. **76**, 2029 (1996).
[56] A. Linnemann *et al.*, Phys. Lett. B **554**, 15 (2003).
[57] A. Voinov *et al.*, Phys. Rev. Lett. **93**, 142504 (2004).
[58] E. Litvinova and N. Belov, Phys. Rev. C **88**, 031302 (2013).
[59] R. Schwengner, S. Frauendorf, and A. C. Larsen, Phys. Rev. Lett. **111**, 232504 (2013).
[60] B. A. Brown and A. C. Larsen, Phys. Rev. Lett. **113**, 252502 (2014).
[61] S. Goriely and E. Khan, Nucl. Phys. A **706**, 217 (2002).
[62] A. J. Koning *et al.*, TALYS-1.4, in *Nuclear Data for Science and Technology*, edited by O. Bersillon, F. Gunsing, E. Bauge, R. Jacqmin, and S. Leray (EDP Sciences, Les Ulis, France, 2008), p. 211, available online at http://www.talys.eu/
[63] A. J. Koning and J. P. Delaroche, Nucl. Phys. A **713**, 231 (2003).
[64] E. Bauge, J. P. Delaroche, and M. Girod, Phys. Rev. C **63**, 024607 (2001).
[65] C. Lederer *et al.*, Phys. Rev. C **83**, 034608 (2011).

[66] P. Zhu, Z. Yuan, J. Chen, Z. Liu, G. Zhang, Z. Shi, and H. Lu, Appl. Radiat. Isot. **65**, 1314 (2007).
[67] V. A. Tolstikov, A. N. Davletshin, E. V. Teplov, O. A. Tipunkov, and O. T. Grudzevich, Yad. Fiz. **58**, 2127 (1995) [Phys. Atomic Nuclei **58**, 2013 (1995)].
[68] A. N. Davletshin, E. V. Teplov, A. O. Tipunkov, V. A. Tolstikov, I. A. Korzh, V. D. Ovdienko, N. M. Pravdivyy, N. T. Sklyar, and V. A. Mishchenko, Vop. At. Nauki i Tekhn., Ser. Yadernye Konstanty **1992**(1), 41 (1992).
[69] A. N. Davletshin, E. V. Teplov, A. O. Tipunkov, S. V. Tikhonov, and V. A. Tolstikov, Vop. At. Nauki i Tekhn., Ser. Yadernye Konstanty **1993**(13), 199303 (1993).
[70] P. Andersson, R. Zorro, I. Bergqvist, M. Herman, and A. Marcinkowski, Nucl. Phys. A **443**, 404 (1985).
[71] J. Voignier, S. Joly, and G. Grenier, Nucl. Sci. Eng. **112**, 87 (1992).
[72] M. Lindner, R. J. Nagle, and J. H. Landrum, Nucl. Sci. Eng. **59**, 381 (1976).